RSC Advances

PAPER

Cite this: *RSC Adv.*, 2016, **6**, 78064

Structural and electronic properties of HC_nS^- (n = 4–11): anion photoelectron spectroscopy and density functional calculations†

Xi-Ling Xu,[ab] Bin Yang,[ab] Hong-Guang Xu,[ab] Xiao-Jiao Deng[ab] and Wei-Jun Zheng*[ab]

We investigated the HC_nS^- (n = 4–11) clusters using anion photoelectron spectroscopy and density functional theory calculations. The partially resolved vibrational spectra of the HC_nS^- (n = 4–11) clusters are obtained. We found that the vertical detachment energies of the HC_nS^- (n = 4–11) clusters display an obvious parity effect with increasing number of carbon atoms: the vertical detachment energies of the even-numbered HC_nS^- are higher than their neighboring odd-numbered counterparts; the spectral features of the even-numbered HC_nS^- are much sharper than those of their odd-numbered counterparts. The ground-state structures of the anionic and neutral HC_nS (n = 4–11) clusters are linear with the H and S atoms locating at two ends of the carbon chain. The electron affinities of the neutral HC_nS (n = 4–11) clusters are determined based on the transitions from the ground states of HC_nS^- anions to the electronic ground states of HC_nS neutral species.

Received 26th May 2016
Accepted 9th August 2016

DOI: 10.1039/c6ra13665f

www.rsc.org/advances

1. Introduction

Sulfur-bearing carbon chains play vital roles in the chemistry of the interstellar medium,[1–7] and they are very important for understanding the physical and chemical conditions in star forming regions and circumstellar envelopes. The C_nS species can interact with hydrogen, which is the most abundant element in the universe, to form H_mC_nS species in the interstellar medium. Hydrogenated carbon–sulfur chains such as H_2CS and HCS^+ have been detected in the interstellar medium by radio astronomy.[8,9] In addition to their astronomic significance, HC_nS species such as HCS (X $^2A'$) and HCCS (X $^2\Pi$) are important reaction intermediates in the formation of sulfur-containing polycyclic aromatic hydrocarbons.[10,11]

The H_mC_nS (m = 1, 2) species were investigated extensively by experiments and theory. The rotational spectra of HC_nS (n = 2–6) and H_2C_nS (n = 4–7) have been investigated *via* Fourier transform microwave spectroscopy.[12–14] The Renner–Teller effect in HC_2S has been analyzed based on its electronic spectra.[15–20] Recently, Maier and coworkers measured the rovibronic energy levels of X $^2\Pi_{3/2}$ ground state of HC_2S using two-color resonant four-wave mixing techniques[21] and reported the A $^2\Pi_{3/2}$ ← X $^2\Pi_{3/2}$ electronic transition of HC_4S by two-color four-wave mixing techniques and cavity ring down spectroscopy.[22,23] Reilly *et al.* investigated HC_4S using dispersed fluorescence spectroscopy.[24] Nakajima *et al.* studied HC_4S and HC_6S by laser induced fluorescence spectroscopy.[25,26] Denisov *et al.* reported the resonant two-color two-photon ionization A $^2\Pi$ ← X $^2\Pi$ spectrum of HC_6S and measured the origin band of A $^2\Pi$ ← X $^2\Pi$ transitions of HC_8S and $HC_{10}S$ by cavity ring down spectroscopy.[27] Liu *et al.* investigated the structures and properties of laser-generated sulfur polycarbon hydride ions ($HC_nS^{\pm}$) using collision-induced dissociation and *ab initio* calculations.[28] Puzzarini investigated the structural and energetic properties of $HCCS^{0/\pm1}$ using CCSD(T) method.[29] Mladenovic *et al.* studied the hyperfine structure of the X $^2\Pi$ electronic state of HCCS.[30,31] Perić *et al.* investigated the X $^2\Pi$ ground state and A $^2\Pi$ excited state of HCCS by means of an extensive *ab initio* approach.[32,33] Flores studied the electronic spectra of HC_nS (n = 2–4) using MCSCF and MRCI methods.[34] Maier and coworkers calculated the spin–orbit constants, dipole moments and carbon–sulfur distances of HC_nS (n = 1–12) in the $^2\Pi$ electronic ground state.[35] Wang *et al.* reported the ground state structures and stabilities of $HC_{2n}S$ (n = 1–5) using B3LYP density functional calculations.[36] Park *et al.* calculated the structures, harmonic frequencies and dipole moments of H_2C_nS (n = 3–9) using density functional theory (DFT) and MP2 methods.[37] Kim and McMahon investigated the electronic structures and rearrangement pathways of C_4H_2S using coupled cluster theory and DFT calculations.[38]

In order to explore the geometric and electronic properties of the HC_nS^- (n = 4–11) clusters, in this work, we report a study on the HC_nS^- (n = 4–11) clusters using anion photoelectron spectroscopy combined with DFT calculations.

---

[a] *Beijing National Laboratory for Molecular Sciences, State Key Laboratory of Molecular Reaction Dynamics, Institute of Chemistry, Chinese Academy of Sciences, Beijing 100190, China. E-mail: zhengwj@iccas.ac.cn; Fax: +86 10 62563167; Tel: +86 10 62635054*

[b] *University of Chinese Academy of Sciences, Beijing 100049, P. R. China*

† Electronic supplementary information (ESI) available. See DOI: 10.1039/c6ra13665f

2. Experimental and theoretical methods

2.1. Experimental method

The experiments were performed using a home-built apparatus consisting of a laser vaporization source, a time-of-flight (TOF) mass spectrometer, and a magnetic-bottle photoelectron spectrometer, which has been described previously.[39] Briefly, the C_nS^- (n = 4–11) cluster anions were generated in the laser vaporization source by laser ablation of a rotating and translating carbon–sulfur mixture disk target (13 mm diameter, C : S mole ratio 4 : 1) with the second harmonic (532 nm) light pulses from a nanosecond Nd:YAG laser (Continuum Surelite II-10), while helium gas with ~4 atm backing pressure seeded with ethylene molecules (~4%) was allowed to expand through a pulsed valve (General Valve Series 9) over the target for generating hydrogenated carbon–sulfur ($H_mC_nS^-$) anions and cooling the formed clusters. The cluster anions were mass-analyzed by the TOF mass spectrometer. The HC_nS^- (n = 4–11) clusters were each mass-selected and decelerated before being photo detached using the third (355 nm) and the fourth (266 nm) harmonic lights of another Nd:YAG laser (Continuum Surelite II-10), respectively. The photo detached electrons were energy-analyzed by the magnetic-bottle photoelectron spectrometer. The photoelectron spectra were calibrated using the spectra of Cu^- and Au^- taken at similar conditions. The energy resolution of the photoelectron spectrometer was approximately 40 meV for the electrons of 1 eV kinetic energy.

2.2. Theoretical method

The geometry optimizations and frequency calculations of HC_nS^- (n = 4–11) and their neutral counterparts were carried out using DFT with the Becke's three-parameter and Lee–Yang–Parr's gradient-corrected correlation hybrid functional (B3LYP).[40,41] The aug-cc-pVTZ[42] basis set is used for H, C, and S atoms. All calculated energies were corrected by the zero-point

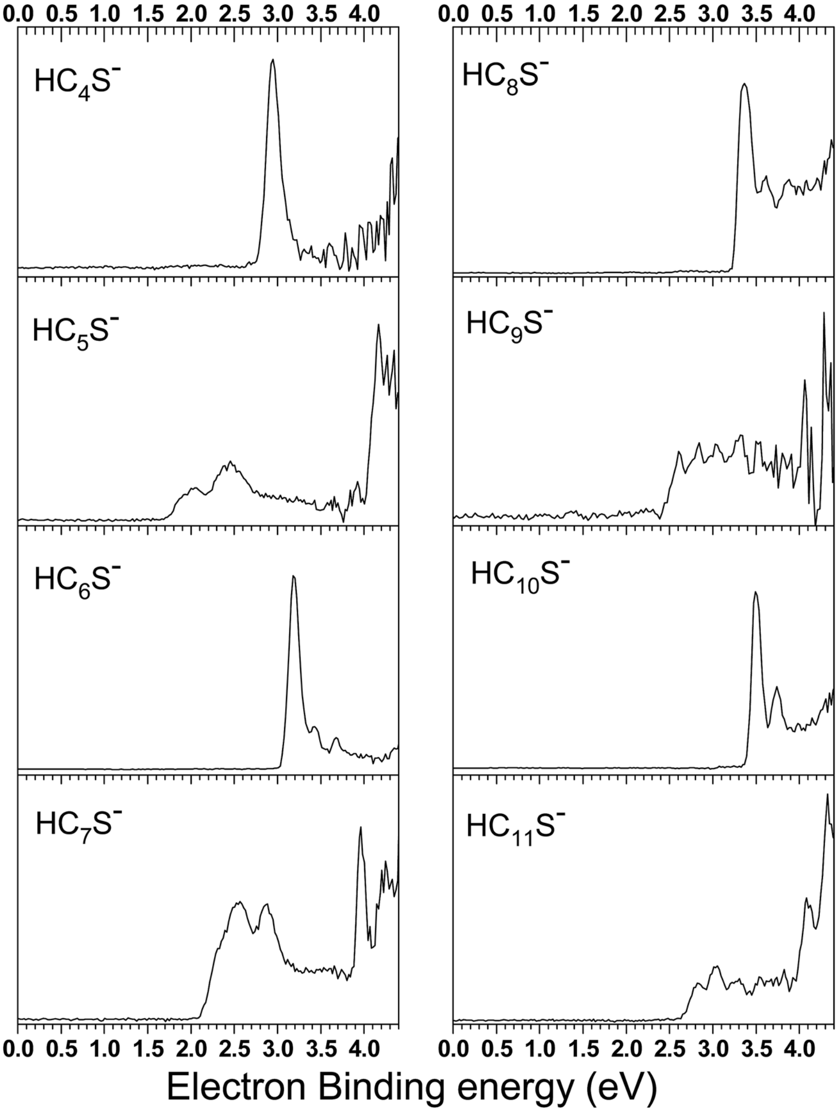

Fig. 1 Photoelectron spectra of HC_nS^- (n = 4–11) recorded with 266 nm photons.

vibrational energies (ZPEs). All the geometry optimizations were conducted without any symmetry constraint. Harmonic vibrational frequencies were calculated to make sure that the optimized structures correspond to real local minima. The theoretical vertical detachment energy (VDE) was calculated as the energy difference between the neutral and anion at the geometry of the anionic species. The theoretical adiabatic detachment energy (ADE) was obtained as the energy difference between the neutral and anion, with the neutral optimized to the nearest local minimum to the anionic geometry. All theoretical calculations in this work were performed with Gaussian 09 program package.[43]

3. Results and discussion

3.1. Experimental results

The photoelectron spectra of HC_nS^- (n = 4–11) taken with 266 nm photons are displayed in Fig. 1. The photoelectron spectra of HC_nS^- (n = 4–7, 9, 11) taken with 355 nm photons are showed in Fig. 2. The 355 nm photoelectron spectra of HC_8S^- and $HC_{10}S^-$ have not been measured because their electron detachment energies reach the limit of 355 nm photon energy in this experiment. The spectra recorded with 266 nm photons show the spectral features of high electron binding energy (EBE), while those at 355 nm give better spectral resolution for the low EBE peaks. The VDEs and ADEs of the HC_nS^- (n = 4–11) clusters obtained from the photoelectron spectra are listed in Table 1. Because the photoelectron spectra of the HC_nS^- (n = 4–11) clusters all have a partially resolved vibrational progression, the VDE of each cluster was taken from the position of the most intensity peak of the vibrational progression, and the ADE of each cluster was determined from the position of the first peak of the vibrational progression.

In the 355 nm spectrum of HC_4S^-, there is one sharp peak centered at 2.93 eV and one small peak centered at 3.18 eV, with a spacing of about 0.25 eV (2020 ± 200 cm^{-1}), which is in good agreement with the vibrational frequency (2007 cm^{-1}) of HC_4S neutral measured by Reilly *et al.*[24] Thus, these peaks can be tentatively assigned to the transitions from the ground state (X $^1\Sigma^+$) of HC_4S^- anion to the vibrational progression of the electronic ground state (X $^2\Pi$) of HC_4S neutral. In the 266 nm spectrum of HC_5S^-, there are three bands centered at 2.05, 2.46, and 4.2 eV, respectively. In the 355 nm spectrum of HC_5S^-, the bands at 2.05 and 2.46 eV are resolved into three peaks centered at 1.97, 2.15, and 2.41 eV. The separation of the first two peaks is 0.18 eV (1450 ± 200 cm^{-1}). These two peaks can be assigned to the transitions from the ground state (X $^3\Sigma^-$) of HC_5S^- anion to the vibrational progression of the electronic ground state (X $^2\Pi$) of HC_5S neutral. The peak at 2.41 eV may come from the contribution of C_5S^- (Fig. S1 in the ESI†) because the mass intensities of HC_5S^- and C_5S^- are similar, thus, $^{13}CC_4S^-$ may contribute ~6% to the mass intensities of HC_5S^-. As for HC_6S^-,

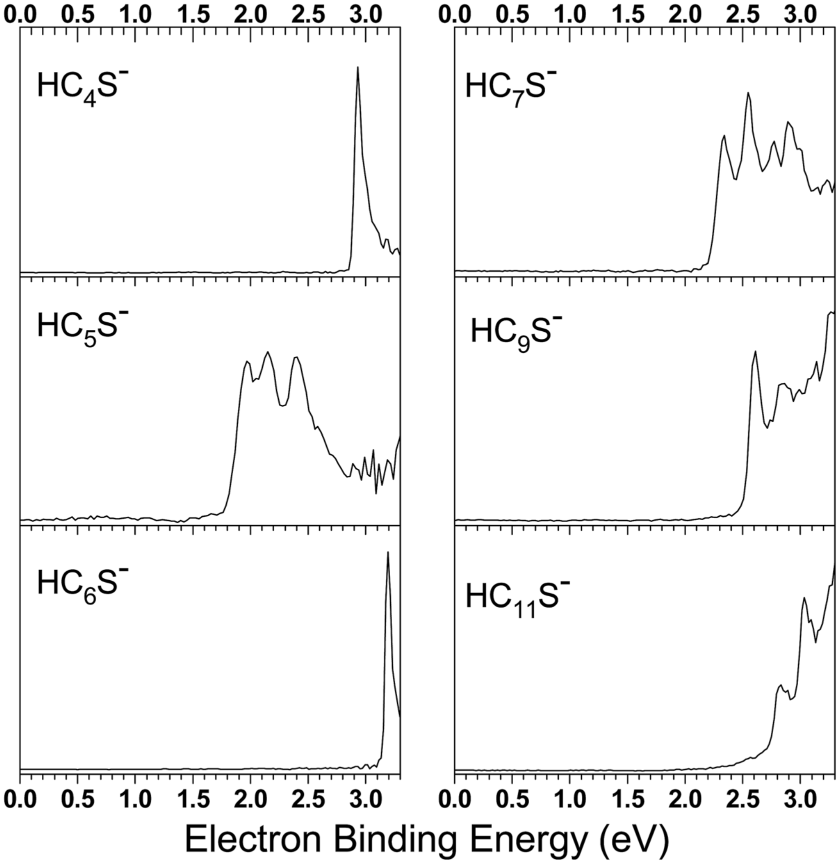

Fig. 2 Photoelectron spectra of HC_nS^- (n = 4–7, 9, 11) recorded with 355 nm photons.

Table 1 Relative energies, theoretical VDEs and ADEs of the low energy isomers of HC_nS^- (n = 4–11), as well as the experimental VDEs and ADEs estimated from their photoelectron spectra. The isomers labeled in bold are the most probable ones in the experiments

					VDE (eV)		ADE (eV)	
Isomer		State	Sym.	ΔE (eV)	Theo.	Expt.[a]	Theo.	Expt.[a]
HC_4S^-	**4A**	$^1\Sigma^+$	$C_{\infty v}$	0.00	2.88	2.93	2.83	2.93
	4B	$^1A'$	C_s	1.86	2.99		2.86	
	4C	$^1A'$	C_s	1.97	3.19		3.10	
HC_5S^-	**5A**	$^3\Sigma^-$	$C_{\infty v}$	0.00	2.25	2.15	2.12	1.97
	5B	$^1A'$	C_s	0.266	2.39		1.84	
	5C	$^1A'$	C_s	0.271	4.14		4.00	
HC_6S^-	**6A**	$^1\Sigma^+$	$C_{\infty v}$	0.00	3.13	3.19	3.09	3.19
	6B	$^1A'$	C_s	1.91	3.25		3.16	
	6C	$^1A'$	C_s	1.94	3.30		3.18	
HC_7S^-	**7A**	$^3\Sigma^-$	$C_{\infty v}$	0.00	2.64	2.55	2.52	2.34
	7B	$^1A'$	C_s	0.37	2.62		2.15	
	7C	$^1A'$	C_s	0.61	4.19		4.12	
HC_8S^-	**8A**	$^1\Sigma^+$	$C_{\infty v}$	0.00	3.33	3.37	3.29	3.37
	8B	$^3A''$	C_s	1.76	1.99		1.53	
	8C	$^1A'$	C_s	1.90	3.48		3.41	
HC_9S^-	**9A**	$^3\Sigma^-$	$C_{\infty v}$	0.00	2.94	2.84	2.83	2.61
	9B	$^1A'$	C_s	0.39	2.67		2.41	
	9C	$^1A'$	C_s	0.84	4.25		4.20	
$HC_{10}S^-$	**10A**	$^1\Sigma^+$	$C_{\infty v}$	0.00	3.47	3.49	3.44	3.49
	10B	$^3A''$	C_s	1.60	2.21		1.84	
	10C	$^1A'$	C_s	1.91	3.66		3.60	
$HC_{11}S^-$	**11A**	$^3\Sigma^-$	$C_{\infty v}$	0.00	3.17	3.05	3.06	2.82
	11B	$^1\Sigma^+$	$C_{\infty v}$	0.42	2.73		2.64	
	11C	$^1A'$	C_s	1.02	3.57		3.52	

[a] The experimental VDEs and ADEs of HC_nS^- with n = 4–7 are estimated from their 355 nm photoelectron spectra, those of HC_nS^- with n = 8–11 are estimated from their 266 nm photoelectron spectra. The uncertainties of the experimental VDEs and ADEs are ±0.05 eV.

there are three resolved peaks centered at 3.19, 3.43, and 3.67 eV respectively. Their spacing is about 0.24 eV (1940 ± 200 cm^{-1}). Similar to HC_4S^-, these peaks correspond to the transitions from the ground state (X $^1\Sigma^+$) of HC_6S^- anion to the vibrational progression of the electronic ground state (X $^2\Pi$) of HC_6S neutral.

In the 266 nm spectrum of HC_7S^-, there are two bands centered at 2.55 and 2.86 eV at the low EBE side, and two more bands centered at 3.96 and 4.3 eV at the high EBE side. In the 355 nm spectrum, the bands at 2.55 and 2.86 eV are resolved into four peaks centered at 2.34, 2.55, 2.77, and 2.89 eV. The spacing of the first three peaks is ~0.22 eV (1770 ± 200 cm^{-1}). These peaks can be assigned to the transitions from the ground state (X $^3\Sigma^-$) of HC_7S^- anion to the vibrational progression of the electronic ground state (X $^2\Pi$) of HC_7S neutral. The 266 nm spectrum of HC_8S^- is composed of three resolved peaks centered at 3.37, 3.62, and 3.87 eV, with a spacing of ~0.25 eV (2020 ± 200 cm^{-1}), which can be assigned to the transitions from the ground state (X $^1\Sigma^+$) of HC_8S^- anion to the vibrational progression of the electronic ground state (X $^2\Pi$) of HC_8S neutral. The 266 nm spectrum of HC_9S^- consists of several resolved peaks centered at 2.61, 2.84, 3.05, 3.30, 3.52, 4.06, and 4.3 eV, respectively. The separation of the first four peaks is ~0.23 eV (1860 ± 200 cm^{-1}), which can be assigned to the transitions from the ground state (X $^3\Sigma^-$) of HC_9S^- anion to the vibrational progression of the electronic ground state (X $^2\Pi$) of HC_9S neutral.

Three peaks centered at 3.49, 3.74, and 3.99 eV are observed in the spectrum of $HC_{10}S^-$, with a spacing of ~0.25 eV (2020 ± 200 cm^{-1}), which can be assigned to the transitions from the ground state (X $^1\Sigma^+$) of $HC_{10}S^-$ anion to the vibrational progression of the electronic ground state (X $^2\Pi$) of $HC_{10}S$ neutral. As for the 266 nm spectrum of $HC_{11}S^-$, it consists of three resolved peaks centered at 2.82, 3.05, and 3.27 eV at the low EBE side, and two sharp peaks centered at 4.09 and 4.33 eV at the high EBE side. The separation of the low EBE features is approximately 0.22 eV (1770 ± 200 cm^{-1}), thus, those three peaks can be assigned to the transitions from the ground state (X $^3\Sigma^-$) of $HC_{11}S^-$ anion to the vibrational progression of the electronic ground state (X $^2\Pi$) of $HC_{11}S$ neutral.

The VDEs of HC_nS^- are lower than those of their C_nS^- counterparts (Fig. S1†), indicating that the addition of an H atom to C_nS^- reduces the VDE. It is worth mentioning that the photoelectron features of HC_6S^- at 3.67 eV, HC_7S^- at 2.89 eV, HC_8S^- at 3.87 eV, HC_9S^- above 3.2 eV, and $HC_{11}S^-$ in the range 3.4–3.9 eV may have minor contributions from C_nS^- because the mass peaks of HC_nS^- have minor contributions from $^{13}CC_{n-1}S^-$. We have confirmed that the contaminations of the spectra are negligible especially at the low electron binding energy side by comparing the spectra of HC_nS^- with those of C_nS^- (n = 4–11),[44,45] which are presented in the ESI (Fig. S1†).

In the spectra of HC_nS^- (n = 4–11), the first peak in each spectrum corresponds to the HC_nS (v' = 0) ← HC_nS^- (v'' = 0) transition, which stands for the ADE of HC_nS^- or the electron affinity (EA) of the neutral HC_nS. For HC_nS^- with even n, the first peaks also correspond to the VDEs of HC_nS^- because the first peak in each spectrum is the most intensity one of the vibrational peaks.

3.2. Theoretical results

We optimized the geometries of the low-lying isomers of HC_nS^- (n = 4–11) and their neutral counterparts. In the calculations, we have considered many different initial structures and multiplicities. The optimized geometries of the low-lying isomers of HC_nS^- (n = 4–11) anions are showed in Fig. 3 with the most stable ones on the left, and those of HC_nS (n = 4–11) neutrals are presented in the ESI (Fig. S2†). The symmetries, relative energies, and theoretical VDEs and ADEs of the low-lying isomers of HC_nS^- (n = 4–11) are listed in Table 1 along with the experimental VDEs and ADEs for comparison. All harmonic vibrational frequencies of the most stable isomers of HC_nS (n = 4–11) neutrals are available in the ESI (Table S1†). We have also simulated the photoelectron spectra of the low-lying isomers of HC_nS^- (n = 4–11) based on theoretically generalized Koopmans' theorem (GKT) and compared the simulated spectra with the experimental results in Fig. 4. For convenience, we call the simulated spectra as density of states (DOS) spectra. Each transition, as the vertical lines in the DOS spectra, corresponds to the removal of an electron from a specific molecular

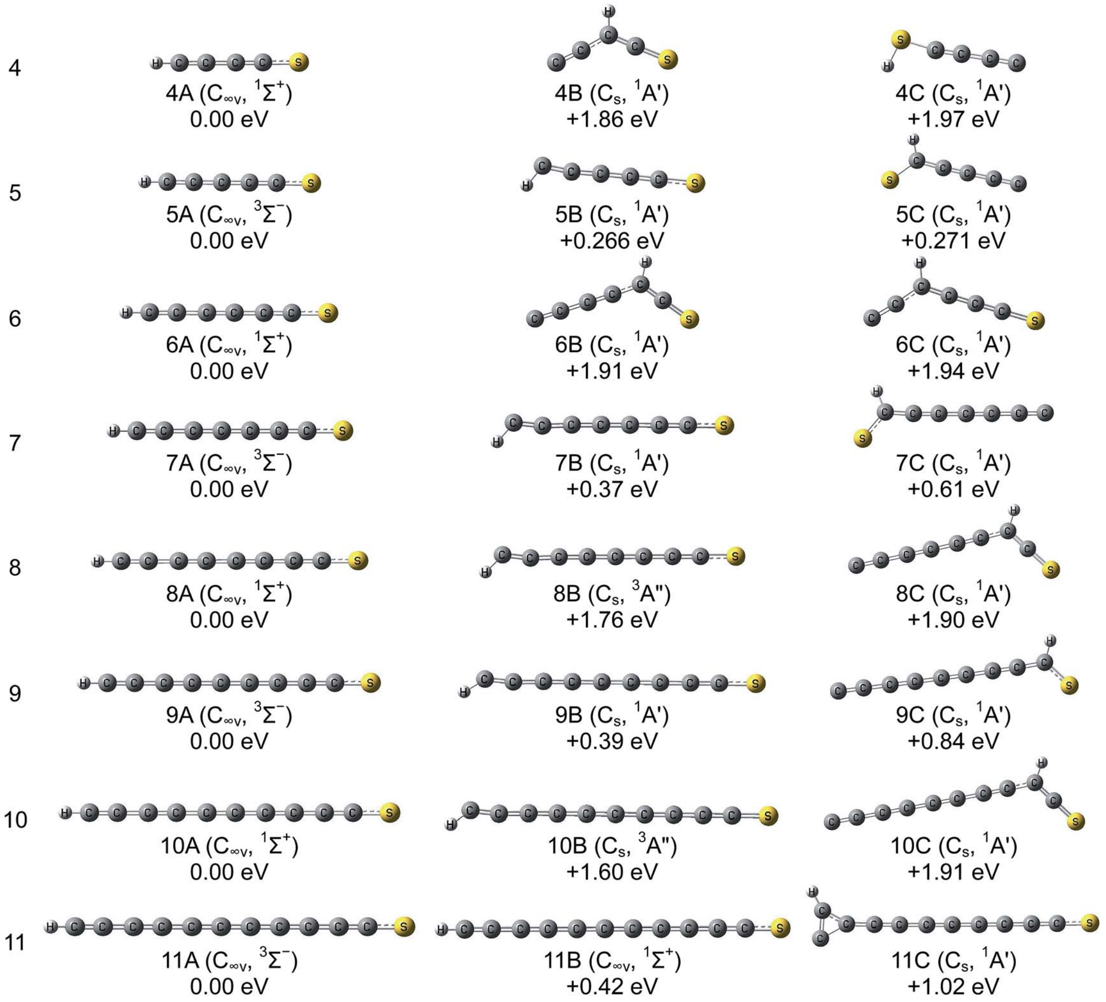

Fig. 3 Geometries, electronic states, and relative energies of the low-lying isomers of HC_nS^- ($n = 4$–11) anions.

orbital of the cluster anion. In the simulation, the first peak associated with the HOMO was set at the position of theoretical VDE, and the other peaks associated with the deeper orbitals were shifted to higher binding energies side according to the relative energies of orbitals (ΔE_n). The values of ΔE_n were calculated by the equation: $\Delta E_n = E_{(\mathrm{HOMO})} - E_{(\mathrm{HOMO}-n)}$, where $E_{(\mathrm{HOMO})}$ is the energy of the HOMO, $E_{(\mathrm{HOMO}-n)}$ is the energy of the HOMO$-n$ orbital from theoretical calculations. The peak associated with each orbital was fitted with a unit-area Gaussian function of 0.2 eV full width at half maximum (FWHM). Note, the DOS spectra only show the transitions related to the electronic states, thus, the vibrational progressions are not displayed in the DOS spectra. The Franck–Condon simulations of the vibrational progression from the electronic ground states of HC_nS^- anions to those of their neutral counterparts were conducted using the ezSpectrum code[46] and are displayed in the ESI (Fig. S3†).

Anionic HC_nS^- ($n = 4$–11). As for HC_4S^-, the most stable isomer (4A) is of $C_{\infty v}$ symmetry with the H and S atoms locating at two ends of the carbon chain. Isomer 4B possesses a V-shaped CC–C–CS chain in which the central C atom interacts with a C═C unit, a C═S unit and one H atom. Isomer 4C is an H–S–C–C–C–C bend structure with a bend of terminal H–S bond. Isomers 4B and 4C are less stable than isomer 4A by 1.86 and 1.97 eV, respectively. The VDE of isomer 4A is calculated to be 2.88 eV, very close to the experimental value (2.93 eV). As we can see from Fig. 4, the simulated DOS spectrum of isomer 4A fits the experimental spectrum very well. Therefore, we suggest that isomer 4A is the most probable one detected in our experiments.

The most stable isomer of HC_5S^- (5A) is a linear structure with a terminal H atom and a terminal S atom. Isomer 5B is an L-shaped structure with a ∠HCC angle of 117° and a terminal S atom. Isomer 5C has a C_5 chain and with the H and S atoms both connecting the terminal C atom of the C_5 chain. The theoretical VDE of isomer 5A is 2.25 eV, in good agreement with the experimental measurement (2.15 eV). Isomers 5B and 5C are much less stable than isomer 5A. Thus, isomers 5B and 5C can be ruled out. In Fig. 4, the simulated DOS spectrum of isomer 5A also agrees with the experimental spectrum. Therefore, isomer 5A is the most probable structure of the HC_5S^- cluster in our experiments.

The lowest-energy structure of HC_6S^- (6A) is a $C_{\infty v}$ symmetric linear structure with the H and S atoms locating at

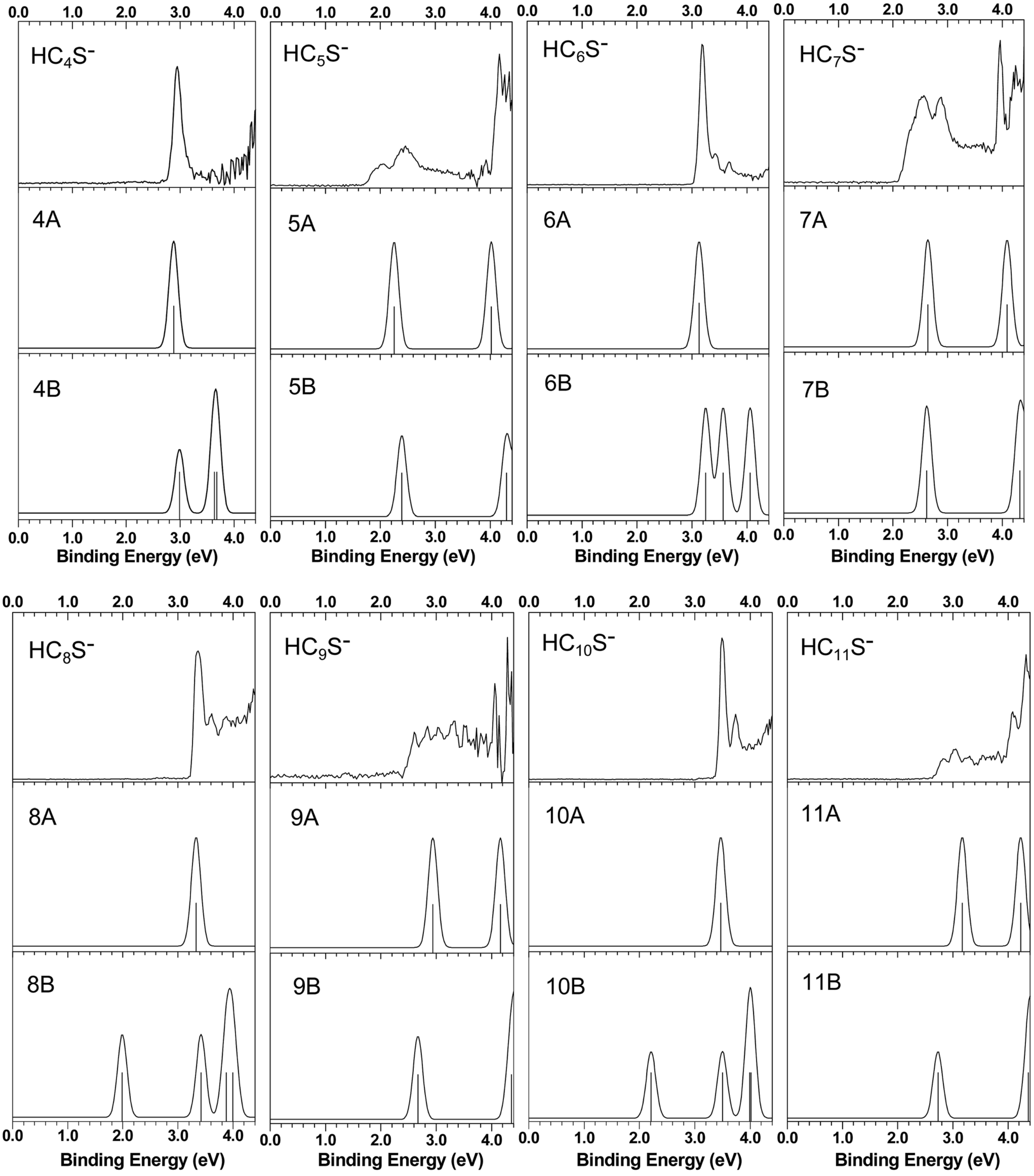

Fig. 4 Comparison of the experimental photoelectron spectra of HC_nS^- ($n = 4–11$) with their simulated DOS spectra. The simulations were conducted by fitting the distribution of the transition lines with unit-area Gaussian functions of 0.2 eV full width at half maximum.

two ends of the C_6 chain. Isomers 6B and 6C are much less stable than isomer 6A by 1.91 and 1.94 eV, respectively. Thus, their existences can be excluded due to their high energies. The theoretical VDE of isomer 6A is 3.13 eV, consistent with the experimental value (3.19 eV). In addition, the simulated DOS spectrum of isomer 6A also agrees with the experimental spectrum in Fig. 4. Therefore, isomer 6A is the most probable species generated in photoelectron spectroscopy experiments.

The most stable isomer of HC_7S^- (7A) is a linear structure with a terminal H atom and a terminal S atom. Isomer 7B is a nonlinear structure with a C_7 chain and a bend of terminal H–C bond. Isomer 7C consists of a carbon chain of C_7 with the H and S atoms both connecting to one terminal C atom of the C_7 chain. Isomers 7B and 7C are higher than isomer 7A by 0.37 and 0.61 eV in energy, respectively. The calculated VDE of isomer 7A is 2.64 eV, in accord with the experimental value (2.55 eV). As we can see from Fig. 4, the DOS spectrum of isomer 7A can fit the experimental spectrum very well. As a result, we suggest that isomer 7A is the most likely structure of HC_7S^- in our experiments.

With respect to HC_8S^-, the lowest-energy structure (isomer 8A) is composed of a C_8 chain, a terminal H–C bond and a terminal C=S bond. Isomer 8B contains a C_8 chain with a bend of terminal H–C bond. Isomers 8B and 8C are much less stable than isomer 8A by 1.76 and 1.90 eV, respectively. The calculated VDE of isomer 8A is 3.33 eV, in excellent agreement with the experimental measurement (3.37 eV). In Fig. 4, the simulated DOS spectrum of isomer 8A is much more similar to the observed spectrum of HC_8S^-. Therefore, isomer 8A is the most probably structure of HC_8S^- detected in our experiments. Isomers 8B and 8C can be ruled out due to their high energies.

The most stable isomer of HC_9S^- (9A) is a $C_{\infty v}$ symmetric linear structure with a terminal H atom and a terminal S atom. Isomer 9B is composed of a C_9 chain with a bend of terminal H–C bond. Isomer 9C consists of a C_9 chain and having the H and S atoms connecting to one terminal C atom of the C_9 chain. Isomers 9B and 9C are higher than isomer 9A by 0.39 and 0.84 eV, respectively. The VDE of isomer 9A is calculated to be 2.94 eV, close to the experimental result (2.84 eV). As we can see from Fig. 4, the DOS spectrum of isomer 9A can fit the experiment spectrum very well. Therefore, we can infer that isomer 9A is most probable one detected in our experiments.

The most stable structure of $HC_{10}S^-$ (isomer 10A) is a linear structure with a C_{10} chain and a terminal H–C bond and a terminal C=S bond. Isomer 10B contains a C_{10} chain with a bend of terminal H–C bond. Isomers 10B and 10C are higher in energy than isomer 10A by 1.60 and 1.91 eV, respectively. The theoretical VDE of isomer 10A is 3.47 eV, in excellent accord with the experimental value (3.49 eV). In Fig. 4, the simulated DOS spectrum of isomer 10A is much similar to the experimental spectrum of $HC_{10}S^-$. Therefore, isomer 10A is the most probable structure of $HC_{10}S^-$ detected in our experiments.

As for $HC_{11}S^-$, the structures of isomers 11A and 11B both are of $C_{\infty v}$ symmetry in different electronic states, in which the H and S atoms locate at two ends of the C_{11} chain. Isomer 11C consists of a triangle of C_3 with the H atom and linear C_8S unit connecting to the two C atoms of C_3 respectively. Isomers 11B and 11C are higher than isomer 11A by 0.42 and 1.02 eV in energy respectively, so their existence can be ruled out in our experiments. The calculated VDE (3.17 eV) of isomer 11A is close to the experimental value (3.05 eV). As we can see in Fig. 4, the simulated DOS spectrum of isomer 11A can fit the experimental spectrum very well. As a result, we suggest that isomer 11A is the most probable one detected in our experiments.

Neutral HC_nS (n = 4–11). We have also calculated the structures of the neutral HC_nS clusters and found the most stable isomers of HC_nS (n = 4–11) neutrals are all $C_{\infty v}$ symmetric linear configurations with the H and S atoms locating at two ends of the C_n chain (Fig. S2†) while the other isomers for each cluster are much less stable than the most stable ones. The bond lengths of the most stable isomers of the anionic and neutral HC_nS (n = 4–11) clusters are displayed in the ESI (Fig. S4†). It can be seen that the C=C and C=S bond lengths are different for the anionic and neutral states. Therefore, it is expected that the breathing-type stretch modes of the neutrals will be excited upon detaching one electron from the anions. For HC_4S neutral, we calculated a vibrational frequency of the breathing-type stretch mode of the carbon chain to be 1979 cm^{-1} (Table S2 in the ESI†). This is in good agreement with the corresponding vibrational spacing of 2020 cm^{-1} observed experimentally in this work and the value of 2072 cm^{-1} calculated by Reilly *et al.*[24] For HC_nS with $n = 5$–11, our calculations show that the vibrational frequencies of the breathing-type stretch modes of the carbon chains are 1678, 1941/2144, 1725/1952, 1905, 1746/1877, 1837/2100, and 1756/1800 cm^{-1}, respectively (Table S2†). These values are all in reasonable agreement with the corresponding vibrational separations of 1450, 1940, 1770, 2020, 1860, 2020, and 1770 cm^{-1} observed experimentally in this work. In addition to the high frequency vibrational modes of the carbon chains, some low frequency vibrational modes could also be excited. However, they cannot be resolved in our experiments due to the limited instrumental resolution.

In summary, the most stable isomers of the anionic and neutral HC_nS (n = 4–11) clusters are all linear structures with the H and S atoms locating at two ends of the C_n chain. We have also considered the HSC_n type of structures with the H atom interacting with the S atom, but found their energies are much higher than the HC_nS type of structures. This is in agreement with the previous calculations of Liu *et al.*[28] Because the most stable structures of HC_nS (n = 4–11) neutrals are similar to those of the corresponding anions, we can estimate the EAs of HC_nS (n = 4–11) neutrals to be 2.93, 1.97, 3.19, 2.34, 3.37, 2.61, 3.49, and 2.82 eV respectively, based on the vibrational resolved spectra of their corresponding anions.

3.3. Discussion

In Fig. 4, we can see from the simulated DOS spectra of HC_nS^- that there is only one electronic state at the low EBE side. That confirms that the low EBE features in the photoelectron spectra of HC_nS^- (n = 4–11) are from the vibrational structures of the electronic ground states of HC_nS neutrals instead of the different electronic states.

In Fig. 1 and 2, we can see that the spectral features of HC_nS^- with even-n are much sharper than those of HC_nS^- with odd-n, indicating that the structure differences between the anion and neutral for HC_nS with even-n is relatively smaller than those of odd-n. For example, the C=S bond of HC_4S^- anion is longer than that of HC_4S neutral by 0.047 Å while the C=S bond of HC_5S^- anion is longer than that of HC_5S neutral by 0.060 Å. In addition, the changes of the C=C bond lengths between HC_4S^- and HC_4S are in the range of 0.004–0.013 Å, much smaller than those (0.015–0.037 Å) between HC_5S^- and HC_5S (Fig. S4†). Fig. 5

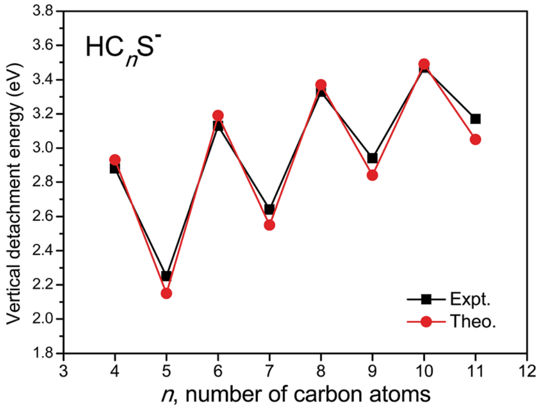

Fig. 5 Experimental and theoretical VDEs of HC$_n$S$^-$ (n = 4–11) *versus* n, the number of carbon atoms.

shows the change of experimental and theoretical VDEs *versus* the number of carbon atoms. It can see that the calculated VDEs are in excellent agreement with the experimental VDEs. The VDEs of the HC$_n$S$^-$ ($n = 4$–11) clusters exhibit the strong odd–even alternation: the VDEs of even-n clusters are higher than those of adjacent odd-n clusters. For HC$_n$S$^-$ ($n = 4$–11) in both odd and even series, the VDEs increase with increasing n. It is worth mentioning that this odd–even alternation of the VDEs for HC$_n$S$^-$ is similar to that observed for C$_n$S$^-$.[44] The odd–even alternation of the VDEs of HC$_n$S$^-$ can also be explained by their electronic configurations. The ground state of HC$_4$S neutral has an electronic configuration π^3 and the formation of a HC$_4$S$^-$ anion produces a close-shell electronic configuration π^4 with a $^1\Sigma^+$ electronic ground state; while the ground state of HC$_5$S neutral has an electronic configuration π^1 and the formation of a HC$_5$S$^-$ anion produces an open-shell electronic configuration π^2 with a $^3\Sigma^-$ electronic ground state. Therefore, the electron affinity of HC$_4$S neutral is higher than that of HC$_5$S neutral. Based on the discussion above, we can infer that the VDEs of HC$_n$S$^-$ with even n are higher than those of adjacent HC$_n$S$^-$ with odd n because the even-numbered HC$_n$S$^-$ have close-shell electronic configurations with fully-occupied π-orbitals while the odd-numbered HC$_n$S$^-$ have open-shell electronic configurations. This odd–even alternation is also in agreement with the observed mass peak pattern for HC$_n$S$^-$ (Fig. S5 in the ESI†): the mass peak intensities of HC$_{\rm n}$S$^-$ with even n are stronger than those of HC$_n$S$^-$ with odd n.

It would be interesting to compare the structures of the HC$_n$S clusters with those of the isovalent HC$_n$O clusters which were investigated in the literature.[47–50] HC$_4$O is reported to have bent planar geometries with a ∠HCC angle of ~160°,[50] which is different from the linear structure of HC$_4$S. The most stable structures of the neutral HC$_n$O ($n = 5$–7) clusters reported in the literature[49] are similar to those of the corresponding neutral HC$_n$S ($n = 5$–7), which all have linear structures with the H and O/S atoms locating at two ends of the C$_n$ chain. The structural difference between HC$_4$O and HC$_4$S is probably because HC$_4$O is subjected to a strong Renner–Teller interaction, resulting in a complete quenching of the orbital angular momentum in a nonlinear molecular structure. The HC$_n$O with $n = 5$–7 are all linear structures, which is because the Renner–Teller interactions are fairly weak and their orbital angular momentums are not quenched.[49]

4. Conclusions

HC$_n$S$^-$ ($n = 4$–11) cluster anions were investigated with anion photoelectron spectroscopy. Their VDEs exhibit a strong odd–even alternation with increasing number of carbon atoms. We observed the partially resolved vibrational progressions of the HC$_n$S$^-$ ($n = 4$–11) clusters. The structures of these cluster anions and their corresponding neutrals were also studied by DFT calculations. We found that the most stable isomers of the anionic and neutral HC$_n$S ($n = 4$–11) clusters are all linear structures with the H and S atoms locating at two ends of the carbon chain. We obtained the EAs of HC$_n$S ($n = 4$–11) neutrals based on the partially resolved vibrational spectra of HC$_n$S$^-$ ($n = 4$–11).

Acknowledgements

This work is supported by the National Natural Science Foundation of China (Grant No. 21303214 and 21273246) and the Knowledge Innovation Program of the Chinese Academy of Sciences (Grant No. KJCX2-EW-H01). The theoretical calculations were conducted on the China Scientific Computing Grid (ScGrid).

References

1 A. A. Penzias, P. M. Solomon, R. W. Wilson and K. B. Jefferts, *Astrophys. J.*, 1971, **168**, L53–L58.
2 J. Cernicharo, M. Gurlin, H. Hein and C. Kahne, *Astron. Astrophys.*, 1987, **181**, L9–L12.
3 N. Kaifu, H. Suzuki, M. Ohishi and T. Miyaji, *Astrophys. J.*, 1987, **317**, L111.
4 S. Saito, K. Kawaguchi, S. Yamamoto, M. Ohishi, H. Suzuki and N. Kaifu, *Astrophys. J.*, 1987, **317**, L115–L119.
5 S. Yamamoto, S. Saito, K. Kawaguchi, N. Kaifu, H. Suzuki and M. Ohishi, *Astrophys. J.*, 1987, **317**, L119–L121.
6 M. B. Bell, L. W. Avery and P. A. Feldman, *Astrophys. J.*, 1993, **417**, L37.
7 M. Agúndez, J. Cernicharo and M. Guélin, *Astron. Astrophys.*, 2014, **570**, A45.
8 M. W. Sinclair, N. Fourikis, J. C. Ribes, B. J. Robinson, R. D. Brown and P. D. Godfrey, *Aust. J. Phys.*, 1973, **26**, 85–91.
9 P. Thaddeus, M. Guelin and R. A. Linke, *Astrophys. J.*, 1981, **246**, L41.
10 R. I. Kaiser, C. Ochsenfeld, M. Head-Gordon and Y. T. Lee, *J. Chem. Phys.*, 1999, **110**, 2391.
11 R. I. Kaiser, M. Yamada and Y. Osamura, *J. Phys. Chem. A*, 2002, **106**, 4825.
12 J. M. Vrtilek, C. A. Gottlieb, E. W. Gottlieb, W. Wang and P. Thaddeus, *Astrophys. J.*, 1992, **398**, L73–L76.
13 Y. Hirahara, Y. Ohshima and Y. Endo, *J. Chem. Phys.*, 1994, **101**, 7342–7349.

14 V. D. Gordon, M. C. McCarthy, A. J. Apponi and P. Thaddeus, *Astrophys. J., Suppl. Ser.*, 2002, **138**, 297–303.

15 C. Bernard, *Can. J. Phys.*, 1985, **63**, 1362.

16 H. Kohguchi, Y. Ohshima and Y. Endo, *Chem. Phys. Lett.*, 1996, **254**, 397.

17 S. G. He and D. J. Clouthier, *J. Chem. Phys.*, 2005, **123**, 014317.

18 S. G. He and D. J. Clouthier, *J. Chem. Phys.*, 2004, **120**, 8544–8554.

19 J. Tang and S. Saito, *J. Chem. Phys.*, 1996, **105**, 8020–8033.

20 E. Kim, H. Habara and S. Yamamoto, *J. Mol. Spectrosc.*, 2002, **212**, 83–88.

21 R. Chauhan, F. J. Mazzotti, R. Raghunandan, M. Tulej, P. P. Radi and J. P. Maier, *J. Phys. Chem. A*, 2010, **114**, 3329–3333.

22 F. J. Mazzotti, E. Achkasova, R. Chauhan, M. Tulej, P. P. Radi and J. P. Maier, *Phys. Chem. Chem. Phys.*, 2008, **10**, 136.

23 F. J. Mazzotti, R. Chauhan, Z. Jamshidi, M. Tulej, P. P. Radi and J. P. Maier, *Mol. Phys.*, 2008, **106**, 2709–2715.

24 N. J. Reilly, G. C. Cupitt, S. H. Kable and T. W. Schmidt, *J. Chem. Phys.*, 2006, **124**, 194310.

25 M. Nakajima, Y. Sumiyoshi and Y. Endo, *Chem. Phys. Lett.*, 2002, **351**, 359–364.

26 M. Nakajima, Y. Sumiyoshi and Y. Endo, *Chem. Phys. Lett.*, 2002, **355**, 116–122.

27 A. Denisov, T. W. Schmidt, A. E. Boguslavskiy, H. Ding, A. Araki and J. P. Maier, *Int. J. Mass Spectrom.*, 2004, **233**, 131–136.

28 Z. Y. Liu, Z. C. Tang, R. B. Huang, Q. Zhang and L. S. Zheng, *J. Phys. Chem. A*, 1997, **101**, 4019.

29 C. Puzzarini, *J. Chem. Phys.*, 2005, **123**, 24313.

30 M. Mladenovic, M. Peric, R. Rankovic and B. Engels, *Mol. Phys.*, 2005, **103**, 587–598.

31 M. Mladenović, M. Perić, S. Jerosimić and B. Engels, *Mol. Phys.*, 2004, **102**, 2623–2634.

32 M. Perić, L. Stevanović and S. Jerosimić, *J. Chem. Phys.*, 2002, **117**, 4233.

33 M. Perić, C. M. Marian and S. D. Peyerimhoff, *J. Chem. Phys.*, 2001, **114**, 6086.

34 J. R. Flores, *J. Phys. Chem. B*, 2003, **107**, 9711–9716.

35 A. Mitrushchenkov, R. Linguerri, P. Rosmus and J. P. Maier, *Mol. Phys.*, 2009, **107**, 1549–1553.

36 S. Wang, J. Li, X. Guo, L. Jiang and J. Zhang, *J. Mol. Struct.: THEOCHEM*, 2009, **900**, 118–120.

37 S. W. Park, K. Park, S. Lee and B. Kim, *Chem. Phys. Lett.*, 2000, **326**, 530–536.

38 Y. S. Kim and R. J. McMahon, *J. Org. Chem.*, 2005, **70**, 8171–8179.

39 H.-G. Xu, Z.-G. Zhang, Y. Feng, J. Y. Yuan, Y. C. Zhao and W. J. Zheng, *Chem. Phys. Lett.*, 2010, **487**, 204–208.

40 C. Lee, W. Yang and R. G. Parr, *Phys. Rev. B: Condens. Matter Mater. Phys.*, 1988, **37**, 785–789.

41 A. D. Becke, *J. Chem. Phys.*, 1993, **98**, 5648.

42 T. H. Dunning, *J. Chem. Phys.*, 1989, **90**, 1007.

43 M. J. Frisch, G. W. Trucks, H. B. Schlegel, *et al.*, *Gaussian 09, Revision A. 02*, Gaussian, Inc., Wallingford, CT, 2009.

44 X. L. Xu, X. J. Deng, H. G. Xu and W. J. Zheng, *Phys. Chem. Chem. Phys.*, 2015, **17**, 31011.

45 To be published. The photoelectron spectra of the C_nS^- ($n = 8–11$) clusters.

46 V. A. Mozhayskiy and A. I. Krylov, *Ezspectrum, version 3.0*, http://iopenshell.usc.edu/downloads, 2008.

47 Y. Endo and E. Hirota, *J. Chem. Phys.*, 1987, **86**, 4319.

48 A. L. Cooksy, J. K. G. Watson, C. A. Gottlieb and P. Thaddeus, *J. Chem. Phys.*, 1994, **101**, 178.

49 S. Mohamed, M. C. McCarthy, A. L. Cooksy, C. Hinton and P. Thaddeus, *J. Chem. Phys.*, 2005, **123**, 234301.

50 H. Kohguchi, Y. Ohshima and Y. Endo, *J. Chem. Phys.*, 1994, **101**, 6463.